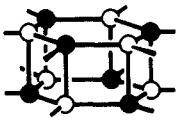

32

between Si atoms, formally Si^{4-}. However, when the electro-

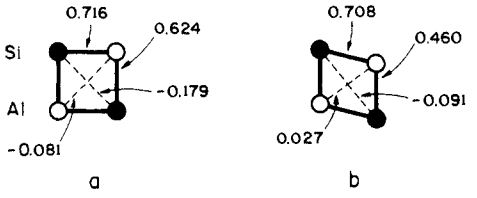

33

negativity difference between the B (open circle) and the X (black circle) atoms is decreased, the repulsion should be minimized. So a stoichiometry of $B_2'B_2^{n-}$ (or $X_2'X_2^{n-}$) should increase the possibility of the "dimerized" graphite structure **32**.

Acknowledgment. We are grateful to the National Science Foundation for its support of this work through Grants CHE 8406119 and DMR 8217227A02 to the Materials Science Center at Cornell University. C. Z. thanks the DFG for a stipend which made his stay in Stuttgart possible. We thank Cora Eckenroth for the typing and Jane Jorgensen for the drawings.

Appendix

The extended Hückel method[35] was used in all calculations. Table II lists the parameters used for Al and Si. The geometry is chosen such that Si is at the center of an idealized Al_4 tetrahedron with Si-Al = 2.45. A 30 k-point set is used in the irreducible wedge in the Brillouin zone[36] to calculate average properties.

(35) Hoffmann, R. *J. Chem. Phys.* **1963**, *39*, 1397; Hoffmann, R.; Lipscomb, W. N. *J. Chem. Phys.* **1962**, *36*, 2179, 3489; **1962**, *37*, 2872. Ammeter, J. H.; Bürgi, H.-B.; Thibeault, J. C.; Hoffmann, R. *J. Am. Chem. Soc.* **1978**, *100*, 3686.

(36) Pack, J. D.; Monkhorst, H. J. *Phys. Rev. B* **1977**, *16*, 1748.

Ligand Effects on the Electronic Structure, Spectra, and Electrochemistry of Tetracobalt Carbonyl Clusters

Gary F. Holland,[1a] Donald E. Ellis,*[1a] and William C. Trogler*[1b]

Contribution from the Department of Chemistry, Northwestern University, Evanston, Illinois 60201, and Department of Chemistry, D-006, University of California at San Diego, La Jolla, California 92093. *Received August 21, 1985*

Abstract: Self-consistent field Xα calculations using the discrete variational method (SCF-Xα-DV) have been performed for $Co_4(CO)_{12}$ (I) and the C_{3v} symmetry model clusters $(\eta\text{-}C_6H_6)Co_4(CO)_9$ (II), $Co_4(CO)_9[(PH_2)_3CH]$ (III), and $(\eta\text{-}C_6H_6)Co_4(CO)_6[(PH_2)_3CH]$ (IV) to explore the effect of phosphine and arene ligands on cluster electronic structures. Density of states plots have been used to simplify analysis of bonding trends in these complex clusters. The cluster core charge varies from 3.11, to 2.58, to 2.41, to 1.80 e along the I-IV series. Charge on the apical Co is least positive in the arene-capped cluster II while basal cobalts are least positive in IV. Ionization potential calculations support qualitative Hückel studies that suggested $(\eta\text{-}C_6H_6)M$ fragments bind more strongly to other metal centers than isolobal $M(CO)_3$ fragments. Electronic absorption spectra of I, $(\eta\text{-}MeC_6H_5)Co_4(CO)_9$ (V), $Co_4(CO)_9$(tripod) (VI) (tripod = $(PPh_2)_3CH$), $(\eta\text{-}MeC_6H_5)Co_4(CO)_6$(tripod) (VII), and $(\eta\text{-}C_6Me_6)Co_4(CO)_6$(tripod) (VIII) exhibit low-energy features between 1000 and 400 nm. Arene-capped clusters exhibit an extra low-energy absorption and calculations for the models II and IV assign this to a HOMO-LUMO transition that resembles intramolecular charge transfer from the apical to basal cobalt atoms. All substituted cobalt clusters V-IX (IX = $(\eta$-[2.2]-paracyclophane$)Co_4(CO)_6$(tripod)) exhibit reversible 1e reductions by cyclic voltammetry. Only clusters VI and VII display reversible 1e oxidations. Redox potentials correlate well with calculated tetracobalt core charges for the model systems I-IV but do not correlate well with HOMO or LUMO energies. Effects of apical and basal substitutions on redox potentials in the tetracobalt clusters are shown to be additive. This supports the notion of delocalized cluster bonding. For this reason cluster core charges better reflect gross properties of the cluster rather than HOMO or LUMO energies of localized two-electron orbitals.

Electronic structures of dinuclear metal complexes have been thoroughly studied,[2] resulting in well-characterized one-dimensional metal-metal interactions. An understanding of the electronic structure of larger clusters,[3] beyond electron counting rules,[4] has not yet been achieved. Trinuclear clusters, which exhibit two-dimensional metal-metal interactions, have been the most extensively studied class of large clusters. Calculations for triangular $M_3(CO)_{12}$ (M = Ru, Os) complexes using extended Hückel theory (EHT)[5] and the self-consistent field Xα discrete

(1) (a) Northwestern University. (b) University of California at San Diego.

(2) (a) Cotton, F. A.; Walton, R. A. "Multiple Bonds between Metal Atoms"; Wiley: New York, 1982. (b) Geoffroy, G. L.; Wrighton, M. S. "Organometallic Photochemistry"; Academic Press: New York, 1979. (c) Lever, A. B. P.; "Inorganic Electronic Spectroscopy"; Elsevier: Amsterdam; 1984.

(3) Manning, M. C.; Trogler, W. C. *Coord. Chem. Rev.* **1981**, *38*, 89-138.

(4) Wade, K. In "Transition Metal Clusters"; Johnson, B. F. G., Ed.; Wiley-Interscience: Chichester, 1980.

(5) (a) Korol'kov, D. V.; Miessner, H. Z. *Z. Phys. Chem.* (*Leipzig*) **1973**, *253*, 25-32. (b) Tyler, D. R.; Levenson, R. A.; Gray, H. B. *J. Am. Chem. Soc.* **1978**, *100*, 7888-7893.

0002-7863/86/1508-1884$01.50/0

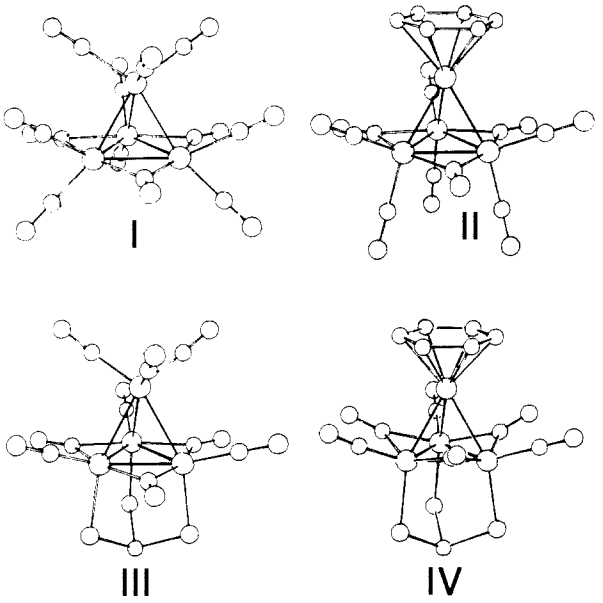

Figure 1. Structures of $Co_4(CO)_{12}$ (I), $(\eta\text{-}C_6H_6)Co_4(CO)_9$ (II), $Co_4(CO)_9[(PH_2)_3CH]$ (III), and $(\eta\text{-}C_6H_6)Co_4(CO)_6[(PH_2)_3CH]$ (IV).

variational method (SCF-Xα-DV)[6] compare favorably with optical[5b] and valence photoelectron[6,7] spectra. Mono- and biscapped triangular clusters of general formulas $(\mu_3\text{-}Y)H_nM_3L_3$ and $(\mu_3\text{-}Y)(\mu_3\text{-}X)H_nM_3L_3$ (n = 0–3; L = $(CO)_3$, C_5H_5) have been examined through EHT[8a] and Fenske–Hall molecular orbital calculations,[9] ultraviolet[10-13] and X-ray[14] photoelectron, optical,[15,16] EPR,[16-20] and nuclear quadrupole resonance (NQR)[21] spectroscopies, as well as with X-ray diffraction[17b,22] and electrochemical techniques.[23-26] Stacked trinuclear Pt clusters have been the subject of recent theoretical[8b] interest.

Increasing cluster nuclearity from three to four generates several possible cluster shapes,[27] including the 60 cluster valence electron (CVE) tetrahedron, the 62 CVE butterfly, and the 64 CVE square plane. A butterfly carbide cluster containing the Fe_4C framework has been the focus of recent theoretical and spectroscopic research[28] owing to the unusual reactivity of the carbide carbon. Electronic properties of tetrametallic cubane clusters have been examined with a variety of theoretical and spectroscopic techniques.[29] For highly symmetrical tetrahedral clusters there are few published theoretical,[30] spectroscopic,[31] and electrochemical papers.[32]

In the context of the metal surface–cluster analogy[33] trinuclear clusters model ligand binding to two-dimensional metallic surfaces. A tetranuclear cluster is the smallest polyhedron to exhibit three-dimensional metal–metal bonding, the first step toward bulk metals. We have recently shown[34] that calculations of magnetic properties for bare M_4 clusters (M = Fe, Co, Ni) parallel trends found for bulk metals. Understanding the relationship between molecular clusters and catalytically active metal particles and bulk metals requires knowledge of the cluster and lattice building blocks and the effects of ligands on the electronic properties of metal localized electronic states.

In this paper we examine the effect of different ligand environments on electronic structure of a common tetrahedral cobalt core with SCF-Xα-DV calculations. In Figure 1 are shown the structures that result when, starting with fully carbonylated $Co_4(CO)_{12}$ (I), three terminal CO's from the apical cobalt are substituted with benzene forming $(\eta\text{-}C_6H_6)Co_4(CO)_9$ (II); one CO from each of the three basal cobalts is substituted by the chelating phosphine $(PH_2)_3CH$ to give $Co_4(CO)_9[(PH_2)_3CH]$ (III), or both substitutions combine to give $(\eta\text{-}C_6H_6)Co_4(CO)_6[(PH_2)_3CH]$ (IV). Theoretical results for these model compounds are compared with spectroscopic and electrochemical measurements for isolable derivatives. Since CO ligation may stabilize metal clusters through delocalization of excess negative charge from the metal core, special attention was directed at determining ligand effects on electron density at the Co_4 core. To reduce the

(6) Delley, B.; Manning, M. C.; Berkowitz, J.; Ellis, D. E.; Trogler, W. C. *Inorg. Chem.* **1982**, *21*, 2247–2253.
(7) Green, J. C.; Mingos, D. M. P.; Seddon, E. A. *Inorg. Chem.* **1981**, *20*, 2595–2602.
(8) (a) Schilling, B. E. R.; Hoffmann, R. *J. Am. Chem. Soc.* **1979**, *101*, 3456–3467. (b) Underwood, D. J.; Hoffmann, R. *J. Am. Chem. Soc.* **1985**, *107*, 5968–5980.
(9) (a) Rives, A. B.; Xiao-Zheng, Y.; Fenske, R. F. *Inorg. Chem.* **1982**, *21*, 2286–2294. (b) Olson, W. L.; Schugart, K. A.; Fenske, R. F.: Dahl, L. F. *Abstr. Pap.—Am. Chem. Soc.* **1984**, *187th*, INOR 279.
(10) (a) Granozzi, G.; Tondello, E.; Ajo, D.; Casarin, M.; Aime, S.; Osella, D. *Inorg. Chem.* **1982**, *21*, 1081–1084. (b) Granozzi, G.; Benoni, R.; Acampara, M.; Aime, S.; Osella, D. *Inorg. Chim. Acta* **1984**, *84*, 95–100.
(11) (a) Chesky, P. T.; Hall, M. B. *Inorg. Chem.* **1981**, *20*, 4419–4425. (b) Sherwood, D. E., Jr.; Hall, M. B. *Organometallics* **1982**, *1*, 1519–1524. (c) Chesky, P. T.; Hall, M. B. *Inorg. Chem.* **1983**, *22*, 2102–2104. (d) Chesky, P. T.; Hall, M. B. *Ibid.* **1983**, *22*, 2998–3007.
(12) (a) Wong, K. S.; Dutta, T. K.; Fehlner, T. P. *J. Organomet. Chem.* **1981**, *215*, C48–C52. (b) DeKock, R. L.; Deshmukh, P.; Dutta, T. K.; Fehlner, T. P.; Housecraft, C. E.; Hwang, J. L.-S. *Organometallics* **1983**, *2*, 1108–1116.
(13) Costa, N. C. V.; Lloyd, D. R.; Brint, P.; Pelin, W. K.; Spalding, R. T. *J. Chem. Soc., Dalton Trans.* **1982**, 201–206.
(14) Xiang, S. F.; Bakke, A. A.; Chen, H.-W.; Eyermann, C. J.; Hoskins, J. L.; Lee, T. H.; Seyferth, D.; Withers, H. P., Jr.; Jolly, W. L. *Organometallics* **1981**, *1*, 699–703.
(15) Geoffroy, G. L.; Epstein, R. A. *Inorg. Chem.* **1977**, *16*, 2795–2799.
(16) Peake, B. M.; Robinson, B. H.; Simpson, J.; Watson, D. J. *Inorg. Chem.* **1977**, *16*, 405–410.
(17) (a) Strouse, C. E.; Dahl, L. F. *Discuss Faraday Soc.* **1969**, *47*, 93–106. (b) Strouse, C. E.; Dahl, L. F. *J. Am. Chem. Soc.* **1971**, *93*, 6032–6041.
(18) (a) Peake, B. M.; Rieger, P. H.; Robinson, B. H.; Simpson, J. *Inorg. Chem.* **1981**, *20*, 2540–2543. (b) Lindsay, P. N.; Peake, B. M.; Robinson, B. H.; Simpson, J.; Honrath, U.; Vahrenkamp, H.; Bond, A. M. *Organometallics* **1984**, *3*, 413–426.
(19) Enoki, S.; Kawamura, T.; Yonezawa, T. *Inorg. Chem.* **1983**, *22*, 3821–3824.
(20) Beurich, H.; Madach, T.; Richter, F.; Vahrenkamp, H. *Angew. Chem., Int. Ed. Engl.* **1979**, *18*, 690–697.
(21) Miller, D. C.; Brill, T. B. *Inorg. Chem.* **1978**, *17*, 240–244.
(22) (a) Stevenson, D. L.; Wei, C. H.; Dahl, L. F. *J. Am. Chem. Soc.* **1971**, *93*, 6027–6031. (b) Byers, L. R.; Uchtman, V. A.; Dahl, L. F. *Ibid.* **1981**, *103*, 1942–1951.
(23) (a) Dessy, R. E.; King, R. B.; Waldrop, M. *J. Am. Chem. Soc.* **1966**, *88*, 5112–5117. (b) Dessy, R. E.; Weissman, P. M.; Pohl, R. L. *Ibid.* 5117–5121.
(24) (a) Bond, A. M.; Peake, B. M.; Robinson, B. H.; Simpson, J.; Watson, D. J. *Inorg. Chem.* **1977**, *16*, 410–415. (b) Bond, A. M.; Dawson, P. A.; Peake, B. M.; Rieger, P. H.; Robinson, B. H.; Simpson, J. *Ibid.* **1979**, *18*, 1413–1417.
(25) Madach, T.; Vahrenkamp, H. *Chem. Ber.* **1981**, *114*, 505–512.
(26) Kotz, J. C.; Peterson, J. V.; Reed, R. C. *J. Organomet. Chem.* **1976**, *120*, 433–437.
(27) Lauher, J. W. *J. Am. Chem. Soc.* **1978**, *100*, 5305–5315; **1979**, *101*, 2604–2607.
(28) (a) Fehlner, T. P.; Housecraft, C. E. *Organometallics* **1984**, *3*, 764–774. (b) Harris, S.; Bradley, J. S. *Ibid.* **1984**, *3*, 1086–1093. (c) Wijeyesekara, S. D.; Hoffmann, R.; Wilker, C. N. *Ibid.* **1984**, *3*, 962–970. (d) Kolis, J. W.; Basolo, F.; Shriver, D. F. *J. Am. Chem. Soc.* **1982**, *104*, 5626–5630. (e) Deshmukh, P.; Dutta, T. K.; Hwang, J. L.-S.; Housecraft, C. E.; Fehlner, T. P. *Ibid.* **1982**, *104*, 1740–1742.
(29) Trinh-Toan; Fehlhammer, W. P.; Dahl, L. F. *J. Am. Chem. Soc.* **1972**, *94*, 3389–3397. Trinh-Toan; Teo, B. K.; Ferguson, J. A.; Meyer, T. J.; Dahl, L. F. *Ibid.* **1977**, *99*, 406–416. Gall, R. S.; Chu, C. T. W.; Dahl, L. F. *Ibid.* **1974**, *96*, 4019–4023. Yang, C. Y.; Johnson, K. H.; Holm, R. H.; Norman, J. G. *Ibid.* **1975**, *97*, 6596–6598.
(30) (a) Hoffmann, R.; Schilling, B. E. R.; Bau, R.; Kaesz, H. D.; Mingos, D. M. P. *J. Am. Chem. Soc.* **1978**, *10*, 6088–6093. (b) Mingos, D. M. P.; Forsyth, M. I. *J. Chem. Soc., Dalton Trans.* **1977**, 610–616. (c) Meissner, H. *Z. Anorg. Allg. Chem.* **1983**, *505*, 187–194. (d) Raatz, F.; Salahub, D. R. *Surf. Sci.* **1984**, *146*, L609–L615.
(31) (a) Plummer, E. W.; Salaneck, W. R.; Miller, J. S. *Phys. Rev. B* **1978**, *18*, 1673–1701. (b) Chini, P. *Pure Appl. Chem.* **1970**, *23*, 489–503. (c) Graff, J. L.; Wrighton, M. S. *J. Am. Chem. Soc.* **1981**, *103*, 2225–2231.
(32) (a) Rimmelin, J.; Lemoine, P.; Gross, M.; de Montauzon, D. *Nouv. J. Chim.* **1983**, *7*, 453–459. (b) Rimmelin, J.; Lemoine, P.; Gross, M.; Bahsoun, A. A.; Osborn, J. A. *Ibid.* **1985**, *9*, 181–188.
(33) Muetterties, E. L.; Rhodin, T. N.; Band, E.; Brucker, C. F.; Pretzer, W. R. *Chem. Rev.* **1979**, *79*, 92–137. Kaesz, H. D. *Chem. Br.* **1973**, *9*, 344–352. Ugo, R. *Catal. Rev.-Sci. Eng.* **1975**, *11*, 225–297.
(34) Holland, G. F.; Ellis, D. E.; Trogler, W. C. *J. Chem. Phys.* **1985**, *83*, 3507–3513.

difficulty in analyzing complex molecular orbital diagrams for large clusters, as well as to illustrate the significance of the results for ligand binding to metal particles, we use a density of states (DOS) analysis for large cluster systems.

Experimental Section

Solvents were obtained from commercial sources, purified by standard methods,[35a] distilled, and stored under N_2. Modified Schlenk (using prepurified N_2) and vacuum line techniques[35b] were used throughout. Dicobalt octacarbonyl, tris(diphenylphosphino)methane (Strem Chemicals), and [2.2]paracyclophane (Aldrich) were used as received. Hexamethylbenzene (Aldrich) was recrystallized from hexanes before use.

Infrared spectra were recorded with a Perkin-Elmer Model PE-283 spectrometer. Optical spectra were recorded on either a PE-320, PE-330, or IBM 9420 spectrophotometer. Samples were contained in a quartz cuvette modified with an attached Teflon valve and Pyrex bulb; all solvents were triply freeze–pump–thaw degassed and vacuum distilled. Electrochemical measurements used a Princeton Applied Research Corp. Model 173 potentiostat/galvanostat with Model 179 digital Coulometer, Model 175 universal programmer, and Model RE0074 X–Y recorder; positive-feedback circuitry was used to compensate for solution resistance. A one-compartment cell (volume 3.5 mL), based on the design of Demortier and Bard,[36] was used in cyclic voltammetry experiments, with a Pt disc working electrode, Pt wire auxiliary electrode (0.020 in.) and Ag wire (0.050 in.) quasi-reference electrode. The Ag quasi-reference (=AgRE) was found to have a potential of +0.31 V vs. SCE; all potentials are reported vs. AgRE unless stated otherwise. Bulk electrolyses were performed in a four-electrode, three-compartment cell modified from a published design.[37] For bulk electrolyses the working electrode was Pt gauze (52 mesh, $^1/_2$ in. × 1 in.); the auxiliary electrode was a coiled Pt wire; the reference electrode was Ag wire. In a typical experiment the supporting electrolyte, tetra-*n*-butylammonium tetrafluoroborate ($TBABF_4$, Aldrich), was weighed in air, transferred to the electrochemical cell, and evacuated overnight at 10^{-5} torr. On a Schlenk line, sample was added to the working compartment against a N_2 flush. The cell was returned to the high-vacuum line and evacuated, and CH_2Cl_2 solvent (from P_2O_5) was distilled into the cell. Volatile materials (e.g., $Co_4(CO)_{12}$) were cooled to 77 K and evacuated before solvent transfer.

The clusters $Co_4(CO)_{12}$,[38] $Co_4(CO)_9$(tripod)[39] (tripod = tris(diphenylphosphino)methane), and (η-MeC_6H_5)$Co_4(CO)_6$(tripod)[39] were prepared according to published procedures.

Synthesis of (η-C_6Me_6)$Co_4(CO)_6$(tripod). By a method analogous to that published for the preparation of (η-arene)$Cr(CO)_3$ compounds,[40] 0.16 g (0.15 mmol) of $Co_4(CO)_9$(tripod) and 0.076 g (0.47 mmol) of C_6Me_6 were dissolved in 30 mL of 5/1 dioxane/THF. The blue-green solution was heated to reflux under a N_2 atmosphere and stirred magnetically; after 5 h the reaction mixture had turned brown. After a total of 20 h of reflux, the brown solution was allowed to cool to room temperature and solvent was removed under vacuum. The brown residue was washed with three 5-mL fractions of hexane, dissolved in CH_2Cl_2, and filtered. A small amount of $Co_4(CO)_9$(tripod) reactant was present (by thin-layer chromatography); washing with 5 mL diethyl ether and recrystallization of the isolated solid from CH_2Cl_2/Et_2O (2:1 v/v) produced lustrous black needles of the title complex in almost quantitative yield: IR(CH_2Cl_2) 1980 m, 1960 s, 1745 m (cm^{-1}). Anal. Calcd for $C_{55}H_{49}O_6P_3Co_4$: C, 58.22; H, 4.35. Found: C, 58.51; H, 4.56.

Synthesis of (η-[2.2]Paracyclophane)$Co_4(CO)_6$(tripod). This complex was prepared as (η-C_6Me_6)$Co_4(CO)_6$(tripod), with recrystallization from CH_2Cl_2/hexane: IR (CH_2Cl_2) 2010 w, 1975 sh, 1950 s, 1735 m (cm^{-1}). Anal. Calcd for $C_{59}H_{47}O_6P_3Co_4$: C, 60.02; H, 3.98. Found: C, 59.81; H, 4.33.

Synthesis of (η-MeC_6H_5)$Co_4(CO)_9$. This complex was prepared from $Co_4(CO)_{12}$ and toluene by using a procedure similar to that outlined above. Refluxing in dioxane/THF under N_2 for 3 h and recrystallizing from hexanes gave air-stable black crystals. Infrared spectral data (cm^{-1}, CH_2Cl_2; 2078 m, 2040 vs, 2005 m, 1833 m, br) agree with published spectra.[41]

Theoretical Methods. Theoretical DV–Xα calculations[42] were performed by using either a Harris 800 or Harris 1000 minicomputer. Numerical atomic orbitals[43] were used as basis functions. For cobalt, all orbitals through 4d were included with a $3d^84s^1$ startup atomic configuration; a potential well[43] was used to localize the diffuse 4p and 4d levels. A minimum basis (1s, 2s, 2p) was adopted for carbon and oxygen; the hydrogen basis consisted of 1s and 2s functions. It was necessary to include orbitals through 3d for phosphorus. Valence orbitals were explicitly orthogonalized against core (through 3p on Co, 1s on C and O, through 2p on P) atomic orbitals. Molecular atomic orbital populations were calculated by using a modified Mulliken scheme.[44] Preliminary calculations were performed by using the self-consistent charge approximation, SCC–Xα–DV.[45] Final calculations of the molecular Coulomb potential used a least-squares fit of the model electron density to the true electron density[42b] evaluated over the same point grid used in the variational (SCF) solutions of the Hartree–Fock–Slater equation.

$$\langle(\rho^{\text{true}} - \rho^{\text{model}})^2\rangle = \text{minimum} \tag{1}$$

The "true" charge density, ρ^{true}, is given (eq 2) by the sum over all j

$$\rho^{\text{true}}(\bar{r}) = \sum_j f_j|\phi_j(\bar{r})|^2 \tag{2}$$

occupied orbitals of occupation number f_j times the square of the molecular wavefunction. The model charge density (eq 3) is expressed as

$$\rho^{\text{model}}(\bar{r}) = \sum_{\nu,n,l} g_{nl}{}^{\nu}|R_{nl}(r_\nu)|^2 \tag{3}$$

an s-wave expansion with overlapping spherical functions on each center, where R_{nl} are the radial atomic basis functions and $g_{nl}{}^{\nu}$ the expansion coefficients for atom ν that best satisfy eq 1. Valence ionization potentials were computed by using spin-restricted transition-state[46] calculations to include relaxation effects. Preliminary calculations showed small relaxation effects for optical transitions. Therefore, optical transition energies were taken from ground-state calculations. Calculations for $Co_4(CO)_{12}$ and (η-C_6H_6)$Co_4(CO)_9$ used bond distances and angles taken from published structures,[47,48] idealized to C_{3v} symmetry. To simplify calculations on the tripod-substituted clusters, phenyl groups were replaced by hydrogen atoms, with a P–H bond length of 1.41 Å.[49] Other parameters were taken from crystal structures of $Co_4(CO)_9$-[$(PPh_2)_3CH$][50] or (η-MeC_6H_5)$Co_4(CO)_9$[$(PPh_2)_3CH$][39] and idealized to C_{3v} symmetry.

The component, or partial, density of states function for atomic basis function j is constructed by weighting each molecular energy level E_n by the corresponding Mulliken population $f_j(n)$ and summing, $D_j(E) = (\Gamma/\pi)\sum_n f_j(n)/[(E - E_n)^2 + \Gamma^2]$, where Γ is a Lorentzian broadening factor[51] (0.4 eV was used in these calculations). The total DOS is found by summing the fragments, $D(E) = \sum_j D_j(E)$.

Results and Discussion

Cluster Electronic Structure Calculations. Self-consistent charge (SCC–Xα–DV) calculations, using Mulliken population analyses of ρ^{true} to derive the molecular Coulomb potential,[45] have proven reliable for predicting relative energies (e.g., optical transitions) in mono- and polynuclear transition-metal complexes.[52] A Coulomb potential produced by least-squares fitting of model densities to the true electron density,[42b] hereafter denoted SCF–Xα–DV (eq 1–3), has been found to yield reliable absolute energies (e.g., first ionization potentials) for both transition-metal and main-group compounds.[53] Addition of multicenter multipolar

(35) (a) Perrin, D. D.; Armarego, W. L. F.; Perrin, D. R. "Purification of Laboratory Chemicals", 2nd Ed.; Pergamon Press: New York, 1980. (b) Shriver, D. F. "Manipulation of Air-Sensitive Compounds"; McGraw-Hill: New York, 1969.
(36) Demortier, A.; Bard, A. J. *J. Am. Chem. Soc.* **1973**, *95*, 3495–3500.
(37) Smith, W. H.; Bard, A. J. *J. Am. Chem. Soc.* **1975**, *97*, 5203–5210.
(38) Chini, P.; Albano, V. G. *J. Organomet. Chem.* **1968**, *15*, 433–440.
(39) Bahsoun, A. A.; Osborn, J. A.; Voelker, C.; Bonnet, J. J.; Lavigne, G. *Organometallics* **1982**, *1*, 1114–1120.
(40) Mahaffrey, C. A. L.; Pauson, P. L. *Inorg. Synth.* **1979**, *19*, 154–158.
(41) Bor, G.; Sbrignadello, G.; Marcati, F. *J. Organomet. Chem.* **1972**, *46*, 357–368.
(42) (a) Painter, G. S.; Ellis, D. E. *Phys. Rev. B* **1970**, *2*, 2887–2898. (b) Delley, B.; Ellis, D. E. *J. Chem. Phys.* **1982**, *76*, 1949–1960.
(43) Averill, F. W.; Ellis, D. E. *J. Chem. Phys.* **1973**, *59*, 6412–6418.
(44) Mulliken, R. S. *J. Chem. Phys.* **1955**, *23*, 1833–1841.
(45) Rosen, A.; Ellis, D. E.; Adachi, H.; Averill, F. W. *J. Chem. Phys.* **1976**, *65*, 3629–3634.
(46) Slater, J. C. "The Self-Consistent Field for Molecules and Solids"; McGraw-Hill: New York, 1974; pp 51–55.
(47) Wei, C. H. *Inorg. Chem.* **1969**, *8*, 2384–2397.
(48) Bird, P. H.; Fraser, A. R. *J. Organomet. Chem.* **1974**, *73*, 103–114.
(49) Norman, J. G., Jr. *J. Chem. Phys.* **1974**, *651*, 4630.
(50) Darensbourg, D. J.; Zalewski, D. J.; Deland, T. *Organometallics* **1984**, *3*, 1210–1217.
(51) Ellis, D. E.; Berkovitch-Yellin, Z. *J. Chem. Phys.* **1981**, *74*, 2427–2435.
(52) Trogler, W. C.; Desjardins, S. R.; Solomon, E. I. *Inorg. Chem.* **1979**, *18*, 2131–2136. Trogler, W. C.; Johnson, C. E.; Ellis, D. E. *Ibid.* **1981**, *20*, 980–986. Trogler, W. C.; Ellis, D. E.; Berkowitz, J. *J. Am. Chem. Soc.* **1979**, *101*, 5896–5901.

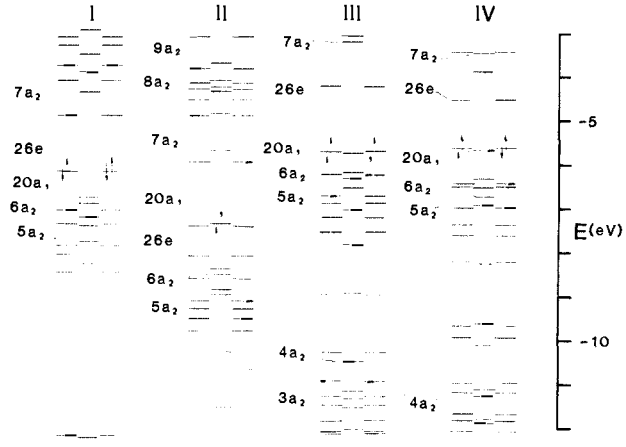

Figure 2. Molecular orbital energy level diagram for clusters I–IV as determined by SCF–Xα–DV calculations.

functions to the least-squares expansion allows calculation of the Coulomb potential to any desired degree of precision.[42b]

Of the clusters under consideration here (Figure 1), valence photoelectron spectra are known only for $Co_4(CO)_{12}$.[7] Calculations of I were used to test the absolute energetic accuracy of our results. The SCF–Xα–DV potentials for $Co_4(CO)_{12}$ (without added fit functions) produced energies that compared well (vide infra) with experimental photoelectron and optical spectra. Since the correlation between theoretical and experimental values for I was good, and in view of the greater computation times required for multipolar corrections to the potential, all cluster calculations reported herein have been performed using a Coulomb potential calculated from a least-squares model without additional correction functions.

Examination of the molecular orbital energy level schemes (Figure 2) reveals a difference between the electronic structures of I and II, III, or IV. In I there is a group of high-energy occupied states separated by a gap (from −8.5 to −12 eV) from lower lying orbitals. Other clusters do not show this segregation of high- and low-energy occupied states. The origin of this gap and the two groups of occupied orbitals is easily understood by using DOS plots where, instead of displaying eigenstates along an energy axis, the density of orbitals, or states, is plotted as a function of energy. These plots have an advantage over molecular orbital energy level schemes because they provide insight into the disposition and composition of orbitals over a broad range of energy. Examination of trends in the energy and makeup of orbitals can be more informative than a tedious level-by-level description for complex molecules.

The total DOS of $Co_4(CO)_{12}$ (Figure 3) sums all individual components contributing to cluster electronic structure. The large separation between peaks at high and low energy for occupied (below the Fermi level) orbitals reflects the gap found in the orbital diagram (Figure 2). The plot goes to a minimum, rather than zero, since an 0.4-eV Lorentzian broadening factor was used in constructing DOS plots. Examination of partial densities of states (PDOS) plots allows assignment of atomic orbital character of peaks in the total DOS plot. The total DOS of I is broken into Co_4 and $(CO)_{12}$ PDOS fragments in Figure 4, which reveals a broad band centered at −7 eV from the tetracobalt core and an intense band at −11 to −16 eV attributable to carbonyls surrounding the cluster. This distribution of metal and carbonyl levels conforms to He(I) and He(II) UPS data[6,7,10-13] for transition-metal carbonyl compounds; predominantly metal-derived orbitals ionize first and then CO localized levels 3–5 eV to higher energy.

Partial DOS plots for clusters II–IV, Figures 5–7, show three features in common with the $Co_4(CO)_{12}$ PDOS. All clusters

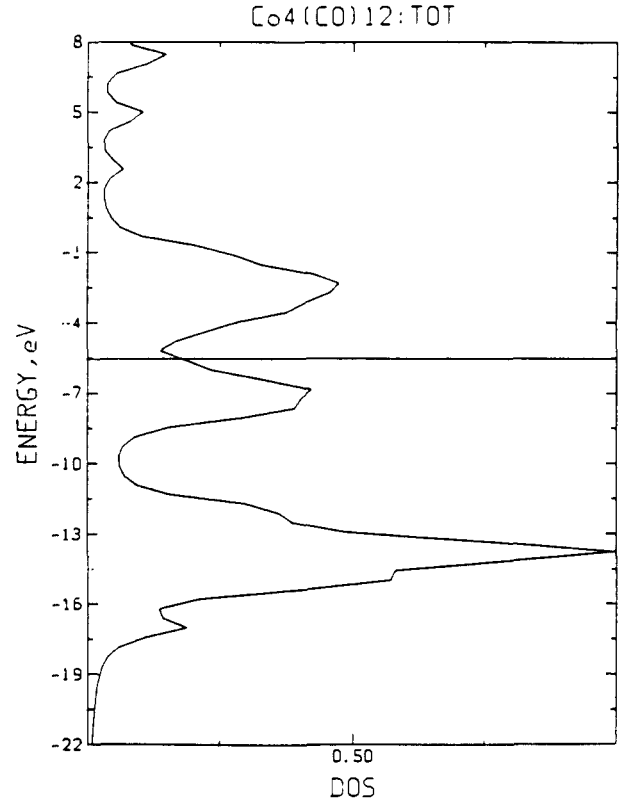

Figure 3. Total density of states (DOS) for $Co_4(CO)_{12}$.

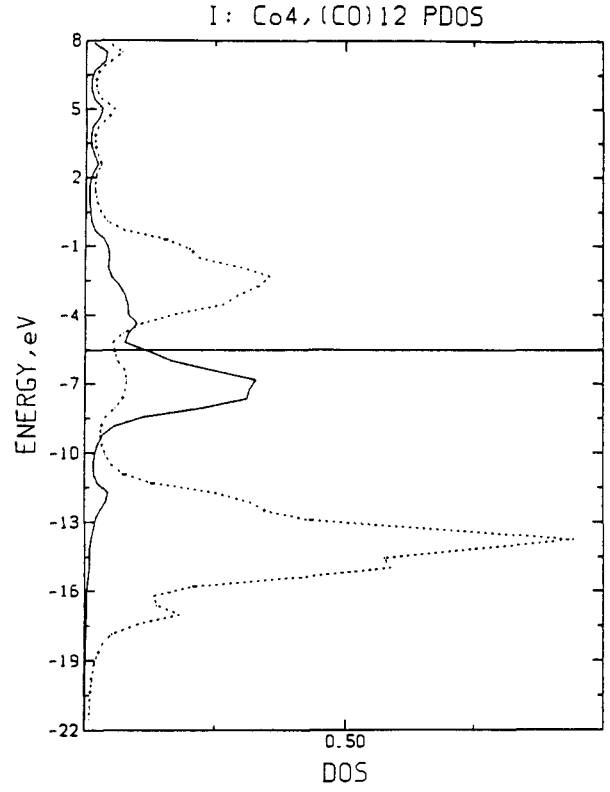

Figure 4. Partial density of states (PDOS) for $Co_4(CO)_{12}$ (I), scaled to total DOS, Figure 3. Note that since an 0.4-eV Lorentzian broadening factor was used in constructing the DOS plots regions where there are no orbitals appear as minima, rather than zero, on the plot: (—) Co_4, (···) $(CO)_{12}$.

exhibit a broad Co_4 peak just below the Fermi energy and two intense carbonyl-based peaks, one near −15 eV and the second just above the Fermi energy. Between the occupied metal and CO bands lie groups of arene and phosphine states. These additional levels lead to the aforementioned difference between the

(53) (a) Holland, G. F.; Manning, M. C.; Ellis, D. E.; Trogler, W. C. *J. Am. Chem. Soc.* **1983**, *105*, 2308–2314. (b) Manning, M. C.; Holland, G. F.; Ellis, D. E.; Trogler, W. C. *J. Phys. Chem.* **1983**, *87*, 3083–3089. (c) Xiao, S.-X.; Trogler, W. C.; Ellis, D. E.; Berkovitch-Yellin, Z. *J. Am. Chem. Soc.* **1983**, *105*, 7033–7037.

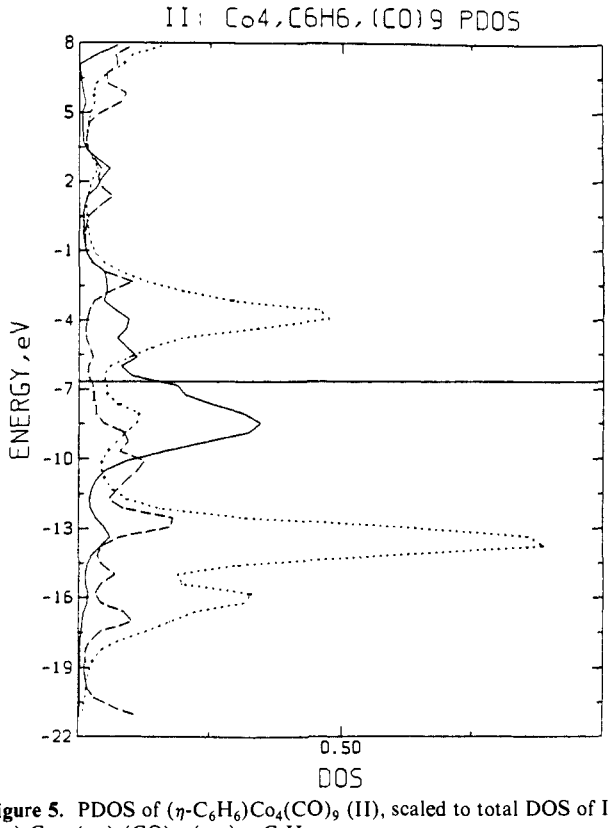

Figure 5. PDOS of $(\eta\text{-}C_6H_6)Co_4(CO)_9$ (II), scaled to total DOS of II. (—) Co_4; (···) $(CO)_9$; (---) $\eta\text{-}C_6H_6$.

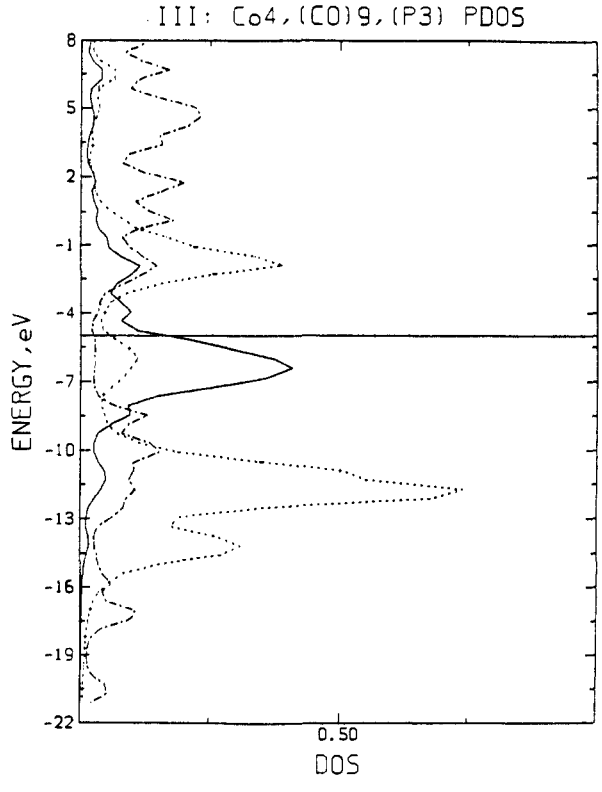

Figure 6. PDOS of $Co_4(CO)_9[(PH_2)_3CH]$ (III), scaled to total DOS of III. (—) Co_4; (···) $(CO)_9$; (---) $[(PH_2)_3CH]$.

gross level structure of I and II–IV.

Three prominent features in the PDOS plots of all four clusters will be discussed first. The lowest energy peaks, with maxima between −11.5 and −14 eV, are carbonyl-localized. A small peak in the cobalt DOS beneath this band reflects M–CO σ bonding. Each cluster exhibits a peak just below the Fermi energy that is of metal character. This peak contains a small CO contribution

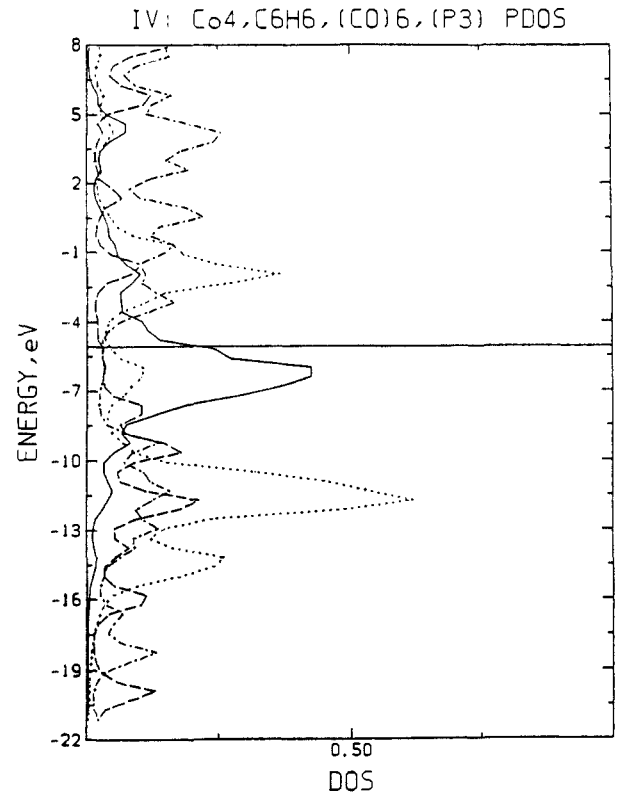

Figure 7. PDOS of $(\eta\text{-}C_6H_6)Co_4(CO)_6[(PH_2)_3CH]$ (IV), scaled to total DOS of IV. (—) Co_4; (···) $(CO)_6$; (---) $\eta\text{-}C_6H_6$; (-·-) $(PH_2)_3CH$.

from $d\pi \rightarrow CO\pi^*$ back-bonding. A large carbonyl-dominated peak just above the Fermi energy has a significant cobalt contribution and corresponds to the $d\pi$–$CO\pi^*$ antibonding set of orbitals. Splitting between the M–$CO\pi^*$ bonding and antibonding peaks varies slightly (I(5 eV)–IV(4.25 eV)) in the PDOS plots for the various clusters.

These plots might seem at odds with the highly covalent nature of metal–CO bonding (as suggested by a referee). While individual metal–CO bonding orbitals (e.g., see Table III) are highly covalent, there are few such orbitals in comparison to the total number in the energy region considered. Thus the plot illustrates that there is a small fraction of metal–CO π bonding orbitals. This should be contrasted with metal hexacarbonyls where all the occupied d orbitals (t_{2g}) bind covalently to CO. The difference arises because metal d orbitals in clusters also participate in metal–metal bonding.

Similar overlap occurs between cobalt and arene or phosphine levels. Occupied π arene states (Figure 5) between −14.5 and −8.5 eV overlap both the metal–CO peak at −13 eV and the broad metal-based band at −9 eV. Other arene contributions are diminished until energies just above the CO–metal peak at −4 eV. The $(PH_2)_3CH$ ligand in III does not contribute significantly to states near the Fermi energy, Figure 6, but the region of −10 to −12 eV contains both M–CO and M–phosphine contributions. Phosphine levels factor significantly into the unoccupied group of states at −2 eV; this dense grouping of states just above the Fermi energy is another mixture of metal, carbonyl, and $(PH_2)_3CH$ orbitals. We attribute this peak to primarily the metal–carbonyl π^* interaction with the phosphine contribution arising from unoccupied P 3d and 3p orbitals. Calculations for various PR_3 derivatives[53c] have shown the importance of unoccupied P 3p orbitals in metal-to-phosphine π-back-bonding. The PDOS for the arene-capped phosphine-substituted cluster, Figure 7, shows a combination of effects discussed above for clusters II and III.

Contribution of metal orbitals to cluster electronic structure may be better understood if the Co_4 PDOS is separated into its 3d, 4s, and 4p components, as in Figure 8 for I. Levels with cobalt 3d contributions span a broad range, from −18 eV to energies well above the Fermi energy. Maximum contribution from 4s and 4p

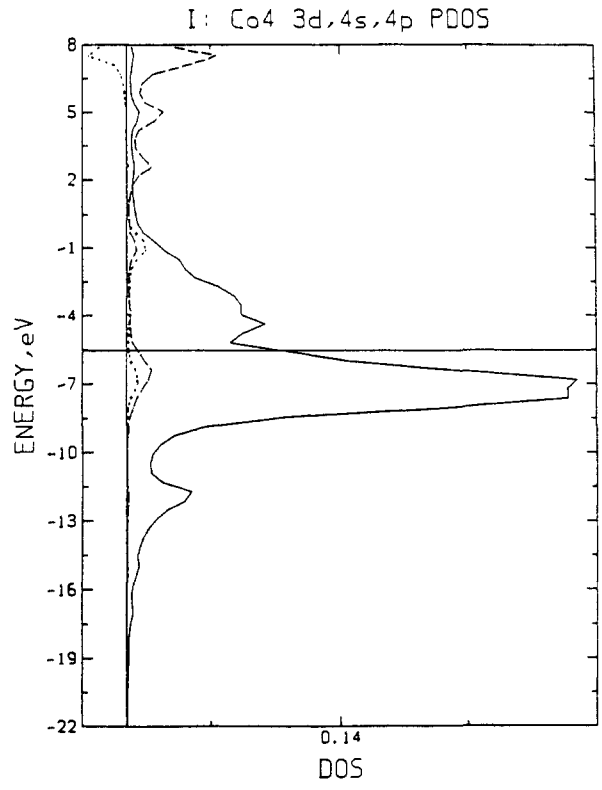

Figure 8. Metal atomic orbital contribution to the Co_4 DOS in $Co_4(CO)_{12}$ (I) scaled relative to total DOS of I. (—) 3d; (···) 4s; (---) 4p.

orbitals to occupied levels occurs in the 3d-dominated region near −7 eV. Clusters II–IV are similar to cluster I in this regard. While the fraction of 4s and 4p character in Co–CO and Co–Co bonding levels is not large, our results appear to be in accord with published EHT calculations,[30] where it was found that the d-orbitals were better suited for metal–metal and metal–carbonyl bonding if small amounts of 4s and 4p orbitals were mixed in.

Cluster Charge Distributions. A detailed description of the charge distribution in these clusters can be obtained from the volume integrated charge around each atom. Here we calculate the charge within the region of space closest to a given atom, as in the Wigner–Seitz construction[54] familiar in the analysis of solids. These values are presented in Table I together with a Mulliken population analysis. We elect to avoid discussion of Mulliken atomic charges because of the extreme basis set dependence of that method. Charge on the apical Co is least positive for the arene-capped case, II, while basal cobalts are least positive in the phosphine substituted cluster IV. Both terminal and bridging carbonyl oxygens carry about the same charge in each cluster, while bridging carbonyl carbons are about 0.1 unit more negative than terminal carbonyl carbons. Since the π^* orbital of CO contains predominant carbon character these charges are a consequence of M–COπ^* back-bonding.

Summing the integrated atomic charges for the metal or ligand atoms allows calculation of cluster fragment charges, Table II. The fully carbonylated cluster core is most positive, +3.11; the apical and basal substituted species II and III exhibit comparable core charges that are less positive than I, +2.58 and +2.41, respectively. Hexasubstituted IV has the least positive core charge of +1.80. As expected, substituting arene and phosphine donors for CO causes less positive charge to build up in the metal core. Bridging carbonyls are calculated more negative than terminal carbonyls, consistent with the observed site preference[55] of Lewis acid binding. The average CO charges are more negative for II, III, and IV than for I, reflecting increased back-bonding because of the added electron density at the metal core.

Integrated charges for benzene and $(PH_2)_3CH$ ligands yield individual atomic volume charges that seem unreasonable, e.g., $P^{+1.94}$, $H^{-0.64}$; however, the total charge for coordinated benzene (+0.54) and $(PH_2)_3CH$ (+1.16) is not unusual for π-and σ-donor ligands. Since the Mulliken population analyses for C_6H_6 and $(PH_2)_3CH$ are much as expected, the apparent difficulty involves the volume-based charge partitioning scheme that assigns a large

Table I. Mulliken Populations, Mulliken Total Charges (Mull), and Volume Integrated Charges ($\int\rho$) for Clusters I–IV

		I	II	III	IV
Co^{apical}	3d	7.70	7.81	7.46	7.76
	4s	0.27	0.28	0.35	0.58
	4p	0.73	0.25	0.87	0.22
	4d	−0.16	−0.18	−0.52	−0.59
Mull		+0.46	+0.84	+0.84	+1.03
$\int\rho$		+0.62	+0.27	+0.58	+0.30
Co^{basal}	3d	7.69	7.68	7.51	7.55
	4s	0.25	0.26	0.39	0.43
	4p	0.39	0.60	0.69	0.88
	4d	−0.30	−0.32	−0.68	−0.66
Mull		+0.97	+0.78	+1.09	+0.80
$\int\rho$		+0.83	+0.77	+0.61	+0.50
C^{apical}	2s	1.30		1.38	
	2p	2.42		2.63	
Mull		+0.28		−0.01	
$\int\rho$		+0.14		+0.11	
$C^{basal,term}$	2s	1.27	1.40	1.45	1.46
	2p	2.63	2.61	2.71	2.73
Mull		+0.10	−0.01	−0.16	−0.19
$\int\rho$		+0.05	+0.05	−0.02	−0.01
O^{term}	2s	1.80	1.82	1.81	1.81
	2p	4.56	4.53	4.57	4.55
Mull		−0.36	−0.35	−0.38	−0.36
$\int\rho$		−0.32	−0.34	−0.40	−0.37
C^{br}	2s	1.34	1.35	1.43	1.42
	2p	2.72	2.77	2.78	2.81
Mull		−0.06	−0.12	−0.21	−0.23
$\int\rho$		+0.02	−0.08	−0.09	−0.12
O^{br}	2s	1.78	1.81	1.81	1.79
	2p	4.55	4.52	4.55	4.54
Mull		−0.33	−0.33	−0.36	−0.33
$\int\rho$		−0.36	−0.39	−0.39	−0.40
C^{π}	2s		1.23		1.31
	2p		3.21		3.26
Mull			−0.44		−0.57
$\int\rho$			+0.68		+0.51
H^{π}	1s		0.43		0.40
	2s		0.06		0.07
Mull			+0.51		+0.53
$\int\rho$			−0.59		−0.48
P	3s			1.64	1.63
	3p			3.32	3.36
	3d			0.33	0.43
Mull				−0.29	−0.42
$\int\rho$				+1.94	+1.60
C^{P}	2s			1.30	1.31
	2p			3.25	3.30
Mull				−0.55	−0.61
$\int\rho$				−0.18	−0.05
H^{P}	1s			0.73	0.70
	2s			0.02	0.02
Mull				+0.25	+0.28
$\int\rho$				−0.64	−0.58

Table II. Volume Integrated Charge of Fragments, Clusters I–IV

fragment	I	II	III	IV
Co_4	+3.11	+2.58	+2.41	+1.80
terminal carbonyl, per CO				
apical	−0.18		−0.29	
basal	−0.27	−0.29	−0.42	−0.38
bridging carbonyl, per CO	−0.34	−0.47	−0.48	−0.52
η-C_6H_6		+0.54		+0.18
$(PH_2)_3CH$, per P			+0.39	+0.23

(54) (a) Slater, J. C. "Symmetry and Energy Bands in Crystals"; Dover Publications: New York, 1972. (b) Charge distributions in cobalt dimers, trimers, and tetramers have been shown[12b] to be chemically significant.

(55) Shriver, D. F. *Chem. Br.* **1972**, *8*, 419–421. Kristoff, J. S.; Shriver, D. F. *Inorg. Chem.* **1974**, *13*, 499–506.

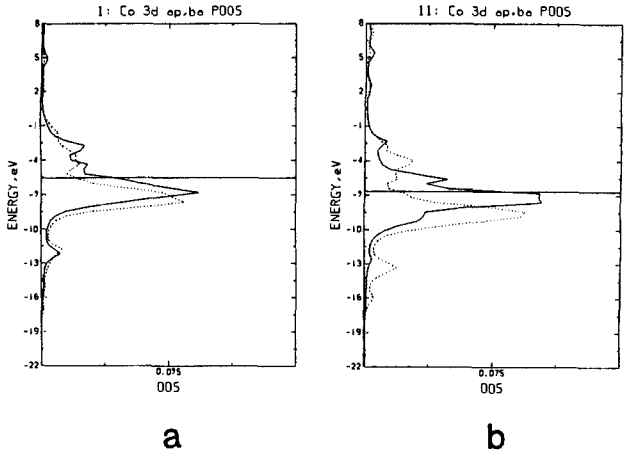

Figure 9. PDOS: Apical and basal site contributions from cobalt 3d orbitals, scaled relative to total DOS and plotted on a per-metal atom basis. (a) $Co_4(CO)_{12}$ (I); (b) $(\eta\text{-}C_6H_6)Co_4(CO)_9$ (II); (—) apical; (···) basal.

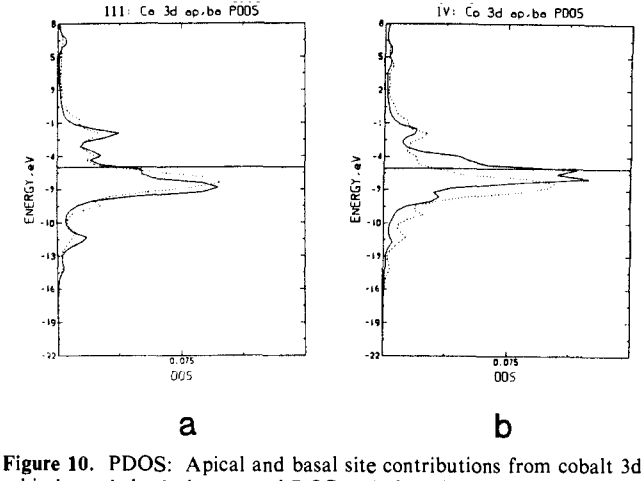

Figure 10. PDOS: Apical and basal site contributions from cobalt 3d orbitals, scaled relative to total DOS and plotted on a per-metal atom basis. (a) $Co_4(CO)_9[(PH_2)_3CH]$ (III); (b) $(\eta\text{-}C_6H_6)Co_4(CO)_6[(PH_2)_3CH]$ (IV); (—) apical 3d; (···) = basal 3d.

region to exterior H atoms and less to the atoms to which H is bound. We are thus reminded of the limitations of any charge-partitioning scheme.

Volume charge analyses explain an unusual feature in the cobalt 3d PDOS. Just as the total DOS was seen to be the sum of its fragment PDOS, and the Co_4 DOS could be separated into 3d, 4s, and 4p components, the Co_4 3d DOS may be further divided into apical and basal contributions. In Figures 9 and 10, the cobalt 3d DOS is plotted on a per atom basis for apical and basal sites in clusters I–IV. The 3d DOS peak corresponding to the site of least positive charge is at higher energy for all clusters except III. It appears that the more positive cobalt site exerts greater Coulombic attraction for its d-electrons, thereby stabilizing them. The less positive site, usually the more substituted one, cannot exercise as great an electrostatic attraction for electrons, and they tend to float closer to the Fermi level. The exception to this trend is the phosphine-substituted cluster III, where the two sites are calculated to be similar in integrated charge, but the more positive (by +0.03) apical cobalt 3d DOS peaks at a slightly higher energy than its basal partner. The reason for this subtle difference is not clearly understood; it is noted, however, that the apical cobalt 3d Mulliken population differs sharply from that of the other clusters.

Similar electrostatic effects may be involved when terminal and bridging carbonyls are considered in Figures 11 and 12. More basic bridging carbonyl levels are generally less bound than terminal CO orbitals. While the charge on the metal core is varied from +3.11 (I) to +1.80 (IV), the gross features of the carbonyl PDOS hardly change. Although bonding in cluster carbonyls is

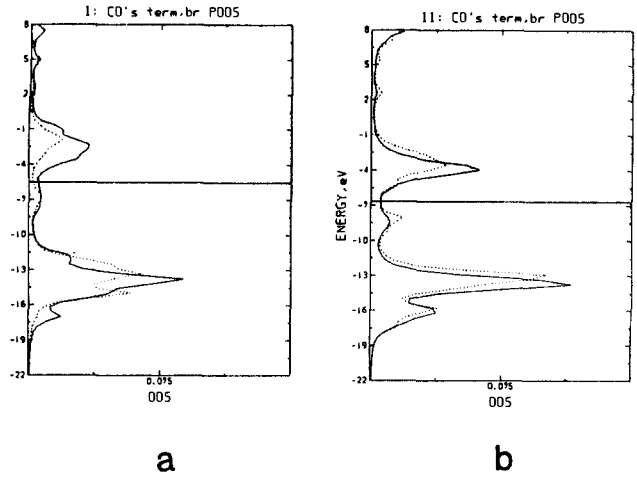

Figure 11. PDOS: Terminal and bridging CO contributions, scaled relative to total DOS and plotted on a per-CO basis. (a) $Co_4(CO)_{12}$ (I); (b) $(\eta\text{-}C_6H_6)Co_4(CO)_9$ (II); (—) terminal; (···) bridging.

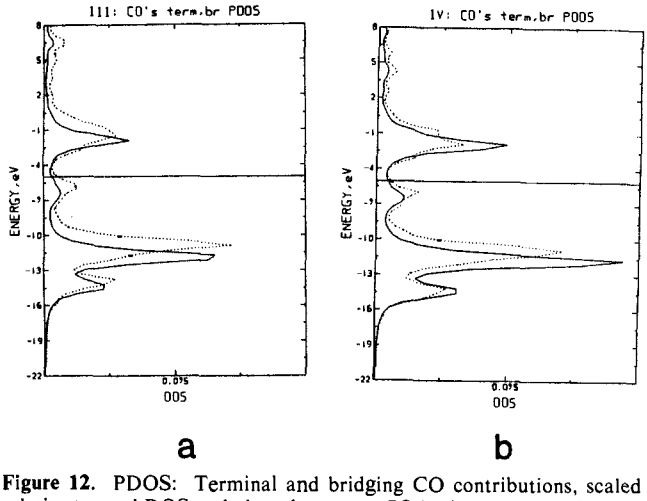

Figure 12. PDOS: Terminal and bridging CO contributions, scaled relative to total DOS and plotted on a per-CO basis. (a) $Co_4(CO)_9[(PH_2)_3CH]$ (III); (b) $(\eta\text{-}C_6H_6)Co_4(CO)_6[(PH_2)_3CH]$ (IV); (—) terminal CO; (···) bridging CO.

delocalized, with large amounts of CO character in metal-based 3d orbitals near the Fermi energy (Table III), the mixing between d and CO levels is not as great as found in mononuclear species.[53a]

Ionization Potentials. There are no published valence photoelectron data for the arene- and phosphine-substituted cobalt clusters II–IV. The He(I) UPS for $Co_4(CO)_{12}$ is known[7] and may be compared with results from SCF–Xα–DV transition-state calculations. The transition-state procedure[46] accounts for some effects of orbital relaxation and is typically about 2 eV for valence orbitals of transition-metal carbonyls. A calculated first IP of 8.19 eV compares well with the UPS spectrum of $Co_4(CO)_{12}$, which exhibits an unresolved band of ionizations with a maximum at 8.9 eV.[7] Spectral broadness of the d ionization band is expected, given the delocalized nature of cluster bonding and high density of states near the Fermi level. If a uniform 2-eV relaxation is assumed for other valence levels, then the total DOS derived from calculations of the first ionization energy serves as a theoretical photoelectron spectrum after making allowance for differences in ionization cross sections. This predicts a broad band of ionizations with a maximum between 9.2 and 9.3 eV, with a second, more intense band at 15.8 eV. The peak of the first band is within 0.4 eV of the experimentally observed value; from ground-state calculations this band is known to be mostly cobalt 3d in character. Peaks at higher energy were obscurred by free CO in the experimental study.[7]

Results of transition-state ionization calculations for clusters I–IV are summarized in Table IV. For each complex the first band ionized is predicted to be metal-centered; a predominantly

Table III. Ground-State Eigenvalues and Fractional Orbital Character for States near Fermi Energy, Clusters I–IV[a]

orbital	*E*, eV	Co^{ap}	Co^{ba}	Ar	CO^{t}	CO^{br}	$(PH_2)_3CH$
$Co_4(CO)_{12}$							
$19a_1$	−6.90	0.03	0.72		0.20	0.05	
$20a_1$	−6.77	0.40	0.29		0.27	0.04	
26e	−6.17*[c]	0.41	0.37		0.20	0.02	
27e	−4.88	0.21	0.46		0.29	0.02	
$7a_2$	−4.35	X[b]	0.29		0.39	0.30	
28e	−4.10	0.03	0.17		0.73	0.02	
$(\pi\text{-}C_6H_6)Co_4(CO)_9$							
26e	−7.39	0.46	0.31	0.11	0.08	0.04	
$20a_1$	−7.36*	0.74	0.17	0.06	0.03		
27e	−5.96	0.35	0.29	0.18	0.15	0.02	
$7a_2$	−5.68	X	0.27		0.27	0.46	
28e	−4.90		0.20		0.66	0.12	
$Co_4(CO)_9[(PH_2)_3CH]$							
$6a_2$	−6.16	X	0.93		0.01	0.03	0.03
$20a_1$	−5.70	0.13	0.44		0.24	0.09	0.10
25e	−5.68*	0.37	0.37		0.17	0.03	0.05
26e	−4.22	0.23	0.49		0.13	0.01	0.13
$7a_2$	−3.21	X	0.24		0.21	0.54	0.01
$21a_1$	−3.05	0.03	0.07		0.10	0.12	0.69
$(\eta\text{-}C_6H_6)Co_4(CO)_6[(PH_2)_3CH]$							
$19a_1$	−6.31	0.15	0.48	0.03	0.14	0.06	0.13
$20a_1$	−5.66	0.70	0.16	0.08	0.05		
25e	−5.60*	0.42	0.35	0.10	0.02	0.04	
26e	−4.52	0.36	0.43	0.09	0.02		
$21a_1$	−3.86	0.02	0.05		0.02	0.06	0.86
$7a_2$	−3.43	X	0.23		0.13	0.62	

[a] Co^{ap} = apical cobalt site; Co^{ba} = basal cobalt site; Ar = coordinated C_6H_6; CO^{t} = terminal carbonyl; CO^{br} = bridging carbonyl. [b] "X" indicates that this site does not contribute to the orbital of concern based on symmetry considerations. [c] * designates the highest occupied molecular orbital (HOMO).

Table IV. Ionization Potentials from SCF–Xα–DV Transition-State Calculations, Clusters I–IV[a]

cluster	1st IP	Δ(gs)[b]	Co band[c]	CO band[d]
I	8.19	2.02	9.2–9.3	15.8
II	9.35	1.99	10.8	15.8
III	7.69	2.01	8.8	14.2
IV	7.64	2.04	8.4	13.7–14.0

[a] All energies in eV. [b] Δ(gs) = relaxation energy of HOMO, measured as the energy difference between HOMO in ground-state and transition-state calculations. [c] Approximate peak of Co_4 based band of ionizations. [d] Approximate peak of carbonyl-based band of ionizations.

carbonyl-localized group of transitions lies between 13 and 17 eV. Between these two ionization regions we predict arene- and phosphine-localized ionizations. These general trends agree well with experimental spectra of related clusters.[6,7,10] Green and co-workers[7] examined several ruthenium, osmium, and rhenium carbonyl clusters and generally observed a band of metal-based ionizations with maxima between 7.5 and 8.0 eV and a carbonyl-localized peak centered at 13.5–15 eV. Studies of tricobalt alkylidyne derivatives by Granozzi et al.[10] showed low-energy metal ionizations near 8–9 eV and large carbonyl-based peaks near 14 eV.

One might expect metal-based ionizations to shift toward lower energy as the cluster core becomes more electron rich through replacement of CO's with arene or phosphine. First IP's for III and IV are calculated less than that of I; however, transition-state calculations for II show 1.5 eV tighter binding than for I. Relaxation effects may be excluded as the origin of tighter binding, since all clusters considered here relax to about the same extent, 2 eV, on ionization. The tighter binding of II compared to I, and IV compared to III suggests that the arene cap plays a significant role in determining absolute cluster energies. Extended Hückel calculations[56] suggest that $(\eta\text{-}C_6H_6)M$ binds more effectively to other metal centers than the isolobal $M(CO)_3$ fragment because of more diffuse frontier orbitals in the former fragment that lead to better overlap. Extending this principle to the clusters considered here we speculate that stronger cap–$Co_3(CO)_9$ bonding for capping $Co(C_6H_6)$ compared to capping $Co(CO)_3$ leads to the anomaly in predicted cluster binding energies. Stronger metal–metal bonding to the Co(arene) cap also helps explain trends in electrochemical properties (vide infra).

Electronic Absorption Spectra. Optical spectra of clusters V–VII (Table V) are better resolved than for I, whose spectrum consists of a broad series of absorptions extending from 900 nm into the UV region, with a peak at 375 nm.[57] The featureless absorption spectrum of I may be understood from Figure 2, since there are a several closely spaced unoccupied levels at low energy.

The calculated optical gap for $Co_4(CO)_{12}$ appears to be underestimated by 0.5 eV. While spectral broadness makes assignment of the experimental HOMO–LUMO transition difficult, we realize that the small basis sets employed in these calculations make accurate prediction of excited-state properties difficult. Addition of virtual 3s, 3p orbitals for carbon and oxygen might yield optical transition energies closer to the experimental value.

Arene-capped clusters V, VII, VIII, and IX each exhibit an intense absorption in the near-IR spectrum, between 870 and 1000 nm. A transition is not observed at this energy in the other clusters and appears to be related to the arene function on the apical cobalt. Eigenfunctions derived from calculations of model clusters II and IV (Table III) show that the highest energy occupied and lowest energy unoccupied levels contain significant amounts of apical cobalt character; contributions from this cobalt site are diminished in orbitals above the LUMO. The HOMO–LUMO transition in II ($20a_1 \rightarrow 27e$) resembles an intramolecular charge transfer, from apical (80% $(\eta\text{-}C_6H_6)Co$) to basal cobalts. Near degeneracy of $20a_1$ and 25e in IV (Figure 2) suggests that a similar excitation may be taking place in this cluster. Little is known about the thermal or photochemical reactivity of complexes containing the $(\eta\text{-arene})Co_4$ fragment.[58] Localization of the HOMO on the apical fragment may lead to interesting arene reactivity.

In the electronic absorption spectrum of $Co_4(CO)_9$(tripod) we assign the shoulder at 760 nm to a (HOMO → LUMO) transition (25e → 26e). The calculated HOMO–LUMO gap for III agrees with the experimental value (within 10%), Table V. Although

(56) Elian, M.; Chen, M. M. L.; Mingos, D. M. P.; Hoffmann, R. *Inorg. Chem.* **1976**, *15*, 1148–1155.

(57) Martinengo, S.; Chini, P.; Albano, V. G.; Cariati, F.; Salvatori, T. *J. Organomet. Chem.* **1973**, *59*, 379–394.

(58) Sisak, A.; Sisak, C.; Ungvary, F.; Palyi, G.; Marko, L. *J. Organomet. Chem.* **1975**, *90*, 77.

Table V. Electronic Absorption Transition Energies[a] and Intensities for Clusters I and V–IX

cluster	λ, nm (ε)	cm^{-1}	eV	calcd eV
$Co_4(CO)_{12}$ (I)	660 (1300)	15200	1.88	1.29
	540 (3000)	19000	2.29	
	460 (5500)	22000	2.69	
	375 (19000)	26700	3.31	
	340 (13000)	29000	3.65	
$(\eta\text{-}MeC_6H_5)Co_4(CO)_9$ (V)	960 (240)	10400	1.29	1.40[b]
	585 (1040)	17100	2.11	
	430 (sh)	23000	2.88	
	385 (11800)	26000	3.22	
	280 (sh)	36000	4.42	
$Co_4(CO)_9$(tripod) (VI)	760 (1100) sh	13200	1.63	1.46[c]
	595 (4590)	16800	2.08	
	450 (4200) sh	22200	2.76	
	380 (11800)	26300	3.26	
	265 (40000) sh	37700	4.68	
$(\eta\text{-}MeC_6H_5)Co_4(CO)_6$(tripod) (VII)	900 (400)	11100	1.38	1.08[d]
	635 (950)	15700	1.95	
	460 (4100)	21700	2.70	
	380 (11200)	26300	3.26	
	320 (13700) sh	31200	3.87	
	260 (30100)	38500	4.78	
$(\eta\text{-}C_6Me_6)Co_4(CO)_6$(tripod) (VIII)	875 (670)	11400	1.42	
	620 (1470)	16100	2.00	
	470 (5330)	21300	2.63	
	385 (14300)	26000	3.22	
	320 (18000) sh	31300	3.87	
$(\eta\text{-}C_{16}H_{16})Co_4(CO)_6$(tripod) (IX)	821 (89)	12300	1.53	
	645 (900) sh	15500	1.92	
	485 (5800) sh	20600	2.56	
	395 (14000)	25300	3.14	
	355 (16000)	28200	3.49	

[a] All spectral data from room temperature, CH_2Cl_2 solution. [b] Calculated value for $(\eta\text{-}C_6H_6)Co_4(CO)_9$. [c] Calculated value for $Co_4(CO)_9[(PH_2)_3CH]$. [d] Calculated value for $(\eta\text{-}C_6H_6)Co_4(CO)_6[(PH_2)_3CH]$.

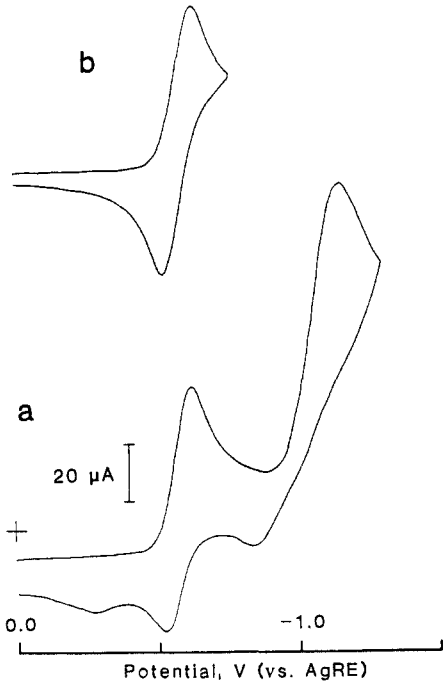

Figure 13. Cyclic voltammogram of 3.5 mM $(\eta\text{-}MeC_6H_5)Co_4(CO)_9$ in CH_2Cl_2/0.2 M $TBABF_4$. Scan rate = 200 mV/s. (a) Potential swept cathodically from 0.00 to −1.30 V; (b) potential swept cathodically from 0.00 to −0.76 V.

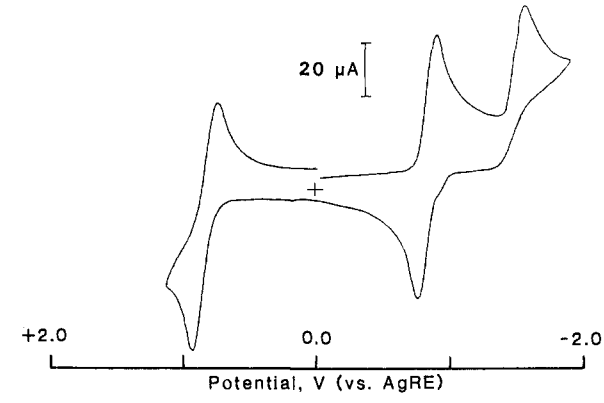

Figure 14. Cyclic voltammogram of 2 mM $Co_4(CO)_9$(tripod) in CH_2Cl_2/0.2 M $TBABF_4$. Scan rate = 200 mV/s. Potential swept first cathodically from 0.00 V, with switching at −1.90 and +1.20 V.

the orbitals involved in the transition are delocalized, they contain mostly (~75%) metal character (Table III). Raman spectral data for $Co_4(CO)_{12}$[59] and related trinuclear clusters[6] show resonance enhancement of the metal–metal stretch on visible wavelength excitation. This suggests the low-energy optical transitions are metal localized. The DOS diagram in Figure 3 shows that phosphine bonding does not contribute significantly to the transition in question, the remaining 25% being of carbonyl character. No reactivity was observed on UV photolysis of $Co_4(CO)_9$(tripod) in the presence of triphenylphosphine; the delocalized nature of the HOMO–LUMO excitation may inhibit photosubstitution.

Electrochemistry. Electrochemical behavior of clusters I and V–IX was studied by using cyclic voltammetry and controlled-potential coulometry. Reversibility of electron transfer in CV experiments was determined through (a) the anodic-to-cathodic peak current ratio, i_{pa}/i_{pc} (=1 for reversible electron transfer) and (b) the separation between cathodic and anodic peak potentials, ΔE_p, compared to the reversible 1e couple ferrocinium/ferrocene either as an internal standard or under identical conditions.[60] Plots of peak current, i_p, vs. $v^{1/2}$ (v = scan rate in V/s) were not linear for these clusters. Similar behavior for ferrocene, together with

(59) Onaka, S.; Shriver, D. F. *Inorg. Chem.* **1976**, *15*, 915–918. Terzis, A.; Spiro, T. G. *J. Chem. Soc., Chem. Commun.* **1970**, 1160–1161.

(60) Gagné, R. R.; Koval, C. A.; Lisensky, G. C. *Inorg. Chem.* **1980**, *19*, 2854–2855.

Table VI. Electrochemical Data[a] for Clusters I and V–IX

cluster	$E°$, V (ΔE_p, mV) n	
	reductns	oxidatns
$Co_4(CO)_{12}$[b] (I)	−0.12 (irrev)	+1.7 (irrev)
$(\eta\text{-}MeC_6H_5)Co_4(CO)_9$ (V)	−0.59 (95) 1, −1.20 (irrev) 2	+1.2 (irrev)
$Co_4(CO)_9$(tripod) (VI)	−0.78 (100) 1, −1.49 (irrev) 1	+0.94 (100) 1
$(\eta\text{-}MeC_6H_5)Co_4(CO)_6$(tripod) (VII)	−1.21 (90) 1	+0.39 (100) 1, +1.2 (irrev)
	−0.85 (100)[c] 1	+0.79 (90)[c] 1
$(\eta\text{-}C_6Me_6)Co_4(CO)_6$(tripod) (VIII)	−1.18 (120) 1	+0.45 (irrev), +1.22 (irrev)
$(\eta\text{-}C_{16}H_{16})Co_4(CO)_6$(tripod) (IX)	−0.88 (120)[c] 1	+0.57 (160)[c]
Cp_2Fe		+0.47 (95)

[a] All data from 0.2 M $TBABF_4/CH_2Cl_2$ solution at 22 °C vs. AgRE unless stated otherwise. [b] Data from 0.2 M $TBABF_4$/THF. [c] Values from 0.1 M $TBABF_4/CH_2Cl_2$ at 22 °C vs. Ag/AgI in 0.1 M $TBAI/CH_3CN$, without compensation for solution resistance.

$\Delta E_p \neq 59$ mV for both clusters and Cp_2Fe, established the presence of some uncompensated solution resistance.

All the substituted tetracobalt clusters V–IX exhibit 1e reductions reversible on the CV time scale at room temperature. Electrochemical data are presented in Table VI, with representative cyclic voltammograms in Figures 13 and 14. Within the potential range available in dichloromethane, only the toluene-capped species V and the tripod substituted cluster IV undergo a second reduction. In addition, clusters VI and VII undergo reversible one-electron oxidations. The unsubstituted cluster $Co_4(CO)_{12}$ did not exhibit reversible electron transfer under the experimental conditions employed (T = 20 °C, scan rate ≤500 mV/s, THF solvent). While reversible reduction of $Co_4(CO)_{12}$ has been observed in 1,2-$C_2H_4Cl_2$ solvent, small amounts of nucleophiles like THF are known[61] to cause fragmentation in clusters of the type $Co_3(CO)_{10}^{2-}$.

Frozen-solution EPR spectra of the reduced clusters of VI and VII at 77 K display one broad (full width = 400 G) signal centered at g = 2.0. Capped trinuclear cobalt clusters of the form $(\mu_3\text{-}Y)Co_3L_3$ (Y = S, Se, CR, PR, $L_3 = C_5H_5$, L = CO)[16-20] have been observed to display complex spectra (up to 22-line EPR spectra) characteristic of the unpaired spin being localized in an orbital of a_2 symmetry. For the tetranuclear cobalt clusters the calculations (Figure 2) suggest the unpaired spin in the radical anion would be localized in an e orbital subject to a Jahn–Teller distortion. Additional couplings arising from inequivalent cobalts and coordinated phosphorus in the tetranuclear tripod cluster may also lead to signal broadening. Low-temperature (4 K) EPR spectra or the use of ENDOR[62] techniques might allow the resolution of hyperfine interactions, where experimentally determined orbital coefficients might be compared with values obtained from Xα–DV calculations.

In a study of $Co_4(CO)_{12}$ and its dppm (dppm = $(PPh_2)_2CH_2$) derivatives, Rimmelin et al.[32a] report for I a reversible one-electron reduction at −0.303 V (vs. SCE) and an irreversible multielectron oxidation at +1.4 V (vs. SCE) using cyclic voltammetry in 1,2-$C_2H_4Cl_2$. The mono- and bis-dppm-substituted clusters also displayed reversible reductions; the bis-dppm cluster exhibited a reversible one-electron oxidation and a second, irreversible one-electron reduction. Furthermore, the bridging phosphine inhibited cluster fragmentation following electron transfer. Independent results for tetracobalt tripod clusters[32b] agree with work reported here and support the findings for the dppm-substituted clusters.

The first reduction for the series of cobalt clusters studied here moves to progressively more negative potentials, I > V > VI > VII. This increasing difficulty in cluster reduction correlates with the decreasing positive charge of the tetracobalt core (Table II) computed for the cluster models. Cluster oxidations follow a similar trend. The reversible oxidation of $(\eta\text{-}MeC_6H_5)Co_4(CO)_6$(tripod) occurs 0.5 V less positive than that of the uncapped tripod cluster; V undergoes an irreversible oxidation at +1.2 V that leads to electrode fouling.

We conclude there is a strong correlation between the calculated charge on the tetracobalt core and the ease of cluster reductions and oxidations. Specifically, less positive cluster cores make reductions more difficult and oxidation easier. There is not as good correlation between HOMO or LUMO energies and the solution redox potentials because of the increased stability of the orbitals for II (Figure 2). A lack of correlation between HOMO energies or IP's and oxidation potentials is surprising since a linear relationship between HOMO energies and oxidation potentials has been reported[63,64] for octahedral metal carbonyl complexes. Metal charges deduced from population analyses did not correlate well in the study of Sarapu and Fenske.[63] Indeed, if we used charges determined by a Mulliken-like procedure, poor correlations were obtained.

Table VII. Linear Correlations for the Electrochemical Behavior of I, V, VI, VII, and VIII

graph plotted	correlation coefficient	slope
$E_{1/2}$(ox) vs. n[a]	0.985	−0.21 ± 0.04
$E_{1/2}$(red) vs. n	0.988	−0.18 ± 0.03
$E_{1/2}$(ox) vs. $\int\rho$[b]	0.997	0.98 ± 0.08
$E_{1/2}$(red) vs $\int\rho$	0.997	0.81 ± 0.07

[a] n = degree of substitution on cluster = 0, 3, or 6 for the complexes examined. [b] $\int\rho$ = volume integrated charge on the Co_4 core in the model clusters I–IV.

A summary of linear correlations, significant at the 99% level,[65] are presented in Table VII. The good linear correlation of volume-integrated metal core charge with degree of subsitution (even with the approximation that the nature of the substituting tripod or arene ligand is irrelevant) shows that ligand effects are additive. This principal has been elegantly developed by Bursten[64] for the prediction of redox potentials of mononuclear carbonyl complexes. Our observations suggest that this theory should be extendable to cluster complexes. Additivity of ligand effects, regardless of the site of substitution, and excellent correlation between net cluster core charges and redox potentials support the notion that metal clusters behave as delocalized sources and sinks of electrons. Lack of correlation between cluster HOMO energies and redox potentials may result because the energy of an individual orbital does not reflect gross molecular properties. Recall that individual cluster orbitals may be localized at apical or basal cobalts or on the ligands. Thus the cluster core charge better represents net effects on cluster bonding. For mononuclear complexes, usually containing metal-localized HOMO's, frontier orbital energies[63,64] may adequately represent metal-centered oxidations and reductions.

Substituted clusters undergo heterogeneous 1e reductions that are reversible on a CV time scale, showing longer lifetimes for reduced species as compared to those produced by reduction of $Co_4(CO)_{12}$. More negative core charges that result from substitution of carbonyls with poor acceptor ligands like arenes and phosphines do not lead directly to cluster instability. Increased stability of the reduced substituted clusters may arise from blocked

(61) Fachinetti, G. *J. Chem. Soc., Chem. Commun.* **1979**, 396–397.
(62) Kurreck, H.; Kirsta, B.; Lubitz, W. *Angew. Chem., Int. Ed. Engl.* **1984**, *23*, 173–194.
(63) Sarapu, A. C.; Fenske, R. F. *Inorg. Chem.* **1975**, *14*, 247–253.
(64) (a) Bursten, B. E. *J. Am. Chem. Soc.* **1982**, *104*, 1299–1304. (b) Bursten, B. E.; Darensbourg, D. J.; Kellogg, G. E.; Lichtenberger, D. L. *Inorg. Chem.* **1984**, *23*, 4361–4365.
(65) Young, H. D. "Statistical Treatment of Experimental Data"; McGraw-Hill: New York; 1962.

Table VIII. Effects of CO Substitution on Bonding in Tetracobalt Clusters[a]

	I[b]	II[c]	VI[d]	VII[e]
$d(Co^{ap}-Co^{ba})$	2.492[a,f]	2.485	2.540	2.472
$d(Co^{ba}-Co^{ba})$	2.492[f]	2.457	2.457	2.447
$d(Co^{ba}-CO^{br})$	2.043	1.948	1.933	1.912
$d(Co^{ap}-CO^{ap})$	1.834[g]		1.793	
$d(Co^{ba}-CO^{t})$	1.834[g]	1.783	1.752	1.740
ν_{CO}, CO^{br}	1868 (pentane)	1829 (hexane)	1780 (CH_2Cl_2)	1740 (CH_2Cl_2)

[a] All distance in Å; ν_{CO} in cm^{-1}. [b] I = $Co_4(CO)_{12}$, from ref 47. [c] II = $(\eta\text{-}C_6H_6)Co_4(CO)_9$, from ref 48. [d] VI = $Co_4(CO)_9$(tripod), from ref 50. [e] VII = $(\eta\text{-}MeC_6H_5)Co_4(CO)_6$(tripod), from ref 39. [f] Average values taken over all Co-Co distances because of disorder in crystal. [g] Average values taken over all Co-to-terminal CO distances because of disorder in crystal.

kinetic pathways to cluster degradation, rearrangement, and substitution. Cyclic voltammetric studies of $Co_4(CO)_{12}$ in THF showed rapid cluster decomposition; no such fragmentation was observed in our studies of tripod-substituted tetracobalt clusters in either THF or CH_2Cl_2. One interpretation of the different electrochemical stabilities of I and tripod derivatives is that the chelating tripod ligand in analogues of III inhibits irreversible metal-metal bond cleavage following electron transfer. Enhanced reversibility in the electrochemical behavior of Co_4 dppm-substituted clusters has also been attributed to bridging ligand effects.[32a] Tripod ligand stabilization of reduced clusters by charge delocalization may be ruled out since ground-state calculations on the clusters $Co_4(CO)_9[(PH_2)_3CH]$ and $(\eta\text{-}C_6H_6)Co_4[(PH_2)_3CH]$ show little $(PH_2)_3CH$ character in the frontier orbitals (Table III).

Bridging of metal-metal bonds with multidentate ligands does not appear to be the sole reason for increased electrochemical stability, since the toluene-capped cluster V is also reduced reversibly. Crystal structure determinations[39,47,48,50] have shown that coordination of an apical arene to a tetracobalt cluster results in the shortening of the apical-basal metal-metal bond,[50] Table VIII. These stronger apical-basal interactions help rationalize the greater electrochemical stability of V and VII compared to I. As mentioned earlier (η-arene)M fragments are better suited to metal-metal bonding than the isolobal $M(CO)_3$ fragment.[56] Donor ligands also cause stronger $(\mu\text{-}CO)Co_2$ interactions through increased metal-to-Co back-bonding, thereby hindering metal-metal bond fragmentation. Stronger metal to bridging CO bonding is suggested by the lower stretching frequency, ν_{CO}, observed in the substituted clusters (Table VIII). The metal-CO distance for bridging carbonyls also decreases with substitution, reflecting a stronger bonding interaction. A similar decrease is seen in terminal carbonyl-metal distances.

Acknowledgment. We thank Dr. J. G. Gaudiello for valuable advice about the electrochemical measurements. This material is based on work supported by the National Science Foundation (Grants DMR82-14966 to D.E.E. and CHE84-02168 to W.C.T.). W.C.T. thanks the Sloan Foundation for a research fellowship.

Pairwise Exchange of Carbon Monoxide in Manganese-Rhenium Decacarbonyl

Steven P. Schmidt,[1a] Fred Basolo,*[1a] Craig M. Jensen,[1b] and William C. Trogler*[1b]

Contribution from the Department of Chemistry, Northwestern University, Evanston, Illinois 60201, and the Department of Chemistry, D-006, University of California at San Diego, La Jolla, California 92093. *Received September 30, 1985*

Abstract: Manganese-rhenium decacarbonyl, selectively enriched on the rhenium atom, is prepared by the rapid reaction between $KMn(CO)_5$ and $Re(^{13}CO)_5(O_3SCF_3)$ that was isotopically enriched to 46%. At temperatures between 65 and 85 °C migration of the label to the Mn atom occurs according to a first-order rate law (k(65 °C) = 0.47 ± 0.09 × 10^{-4} s^{-1}). The reaction is monitored by low-temperature ^{13}C NMR spectroscopy: $Mn-C_{ax}$ δ 215.4; $Mn-C_{eq}$ δ 220.4; $Re-C_{ax}$ δ 179.6; $Re-C_{eq}$ δ 190.5. Activation parameters ($\Delta H^{\ddagger}$ = 12.7 ± 1.4 kcal/mol, $\Delta S^{\ddagger}$ = −41 ± 6 cal/(mol K)), in particular the large negative entropy, are consistent with a pairwise CO exchange mechanism.

Dimanganese, dirhenium, and manganese-rhenium decacarbonyl are prototypical compounds for examining the mechanisms of reaction of metal-metal bonded carbonyls. Carbonyl substitution reactions generally proceed by CO dissociation,[2-5] however, metal-metal bond homolysis has been observed[6] for certain phosphine-substituted manganese dimers. Oxidation reactions of the metal-metal bond take place by both inner- and outer-sphere mechanisms.[7] Irradiation of the parent carbonyls with ultraviolet light leads to metal-metal bond homolysis and the production of 17-electron radical intermediates.[8] Carbonyl-bridged intermediates have been proposed[5] to explain anomalous product distributions in substitution reactions of $MnRe(CO)_{10}$ as well as for photochemical reactions of metal cluster compounds in which the metal-metal bond may be broken.[9] Irradiation of

(1) (a) Northwestern University. (b) University of California at San Diego.
(2) Basolo, F.; Wawersik, H. *Inorg. Chim. Acta* **1969**, *3*, 113-120.
(3) Schmidt, S. P.; Trogler, W. C.; Basolo, F. *Inorg. Chem.* **1982**, *21*, 1698-1699.
(4) Muetterties, E. L.; Burch, R. R.; Stolzenberg, A. M. *Annu. Rev. Phys. Chem.* **1982**, *33*, 89-118.
(5) Sonnenberger, D.; Atwood, J. D. *J. Am. Chem. Soc.* **1980**, *102*, 3484-3489.
(6) Poë, A.; Sekhar, C. V. *J. Am. Chem. Soc.* **1985**, *107*, 4874-4883.
(7) Schmidt, S. P.; Trogler, W. C.; Basolo, F. *J. Am. Chem. Soc.* **1984**, *106*, 1308-1313. Schmidt, S. P.; Trogler, W. C.; Basolo, F., to be submitted.
(8) Wrighton, M. S.; Ginley, D. S. *J. Am. Chem. Soc.* **1975**, *97*, 2065-2072. Kidd, D. R.; Brown, T. L. *J. Am. Chem. Soc.* **1978**, *100*, 4095-4103.
(9) Desrosiers, M. F.; Ford, P. C. *Organometallics* **1982**, *1*, 1715-1716. Malito, J.; Markiewitz, S.; Poë, A. *Inorg. Chem.* **1982**, *21*, 4335-4337. Desrosiers, M. F.; Wink, D. A.; Ford, P. C. *Inorg. Chem.* **1985**, *24*, 1-2.

0002-7863/86/1508-1894$01.50/0